Spatially and Temporally Synchronized Atomic Force and Total Internal Reflection Fluorescence Microscopy for Imaging and Manipulating Cells and Biomolecules

Miklós S. Z. Kellermayer,* Árpád Karsai,* András Kengyel,* Attila Nagy,* Pasquale Bianco,* Tamás Huber,* Ágnes Kulcsár,† Csaba Niedetzky,‡ Roger Proksch,§ and László Grama*

*Department of Biophysics, University of Pécs, Faculty of Medicine, Pécs H-7624, Hungary; †Institute of Physical Chemistry, University of Heidelberg, 69120 Heidelberg, Germany; ‡Supertech Ltd., Pécs H-7624, Hungary; and §Asylum Research, Santa Barbara, California 93117

ABSTRACT The atomic force microscope is a high-resolution scanning-probe instrument which has become an important tool for cellular and molecular biophysics in recent years but lacks the time resolution and functional specificities offered by fluorescence microscopic techniques. To exploit the advantages of both methods, here we developed a spatially and temporally synchronized total internal reflection fluorescence and atomic force microscope system. The instrument, which we hereby call STIRF-AFM, is a stage-scanning device in which the mechanical and optical axes are coaligned to achieve spatial synchrony. At each point of the scan the sample topography (atomic force microscope) and fluorescence (photon count or intensity) information are simultaneously recorded. The tool was tested and validated on various cellular (monolayer cells in which actin filaments and intermediate filaments were fluorescently labeled) and biomolecular (actin filaments and titin molecules) systems. We demonstrate that with the technique, correlated sample topography and fluorescence images can be recorded, soft biomolecular systems can be mechanically manipulated in a targeted fashion, and the fluorescence of mechanically stretched titin can be followed with high temporal resolution.

INTRODUCTION

The atomic force microscope (AFM) is a high-resolution scanning-probe device in which a sharp tip at the end of a flexible cantilever is scanned across a surface (1). In the past decade AFM has been increasingly used in biological applications owing to improvements in sample preparation, development of different data acquisition modes (noncontact mode) and experimental geometries (e.g., force spectroscopy (2)), and the ability of functionalizing the AFM tip that interacts with the sample (3).

There have been numerous attempts to combine AFM with fluorescence imaging (4–6). The motivation for combining AFM with fluorescence arises from the desire to exploit the complementary advantages of both techniques. Whereas AFM provides high spatial resolution and the possibility of mechanical manipulation, fluorescence offers high temporal resolution, sensitivity to local physical chemistry, and the possibility of functional imaging via specific labeling procedures. Imaging with combinations of AFM and various fluorescence microscopies (epifluorescence, confocal, total internal reflection fluorescence (TIRF)) have most often been sequential rather than simultaneous, owing to the difficulties in geometric arrangement and grossly different acquisition timescales. TIRF microscopy (TIRFM) (7), due to the narrow excitation field and its ability to detect and follow individual fluorophores, may offer special advantages in AFM-fluorescence combinations. Recently, individual green fluorescent protein (GFP) molecules picked up by an AFM cantilever tip were imaged with TIRFM (8), and simultaneous force and fluorescence measurements were achieved by following the emission of a fluorescent microsphere glued to a cantilever tip and excited with a calibrated evanescent field (9).

In this work, we developed a spatially and temporally synchronized TIRF (STIRF) and AFM system. The instrument was validated and tested on various cellular and biomolecular systems. With the technique, it is possible to correlate topography and fluorescence features of the examined specimen to mechanically manipulate soft biomolecular samples in a targeted fashion and to follow changes in the fluorescence properties of mechanically stretched biomolecules with high time resolution.

MATERIALS AND METHODS

Protein purification and fluorescent labeling

Actin (10), myosin (11), heavy meromyosin (HMM) (12), and titin (13) were purified according to established methods. F-actin was fluorescently labeled with molar excess of tetramethylrhodamine-isothiocyanate-phalloidin (TRITC-phalloidin, Sigma, St. Louis, MO). Titin was labeled with ~100× molar excess of tetramethylrhodamine iodoacetamide (TMRIA) or Oregon Green 488 maleimide (Molecular Probes, Eugene, OR) (14). Unbound fluorophores were removed by gel filtration (CL-2B Sepharose).

Actin-filament imaging

To image actin, fluorescently labeled filaments were immobilized on a surface coated with HMM (12,13,15). Briefly, a 24 × 60-mm glass coverslip (No. 1) was coated with 1% nitrocellulose (in isoamylacetate, Fullam,

Submitted March 20, 2006, and accepted for publication July 6, 2006.

Address reprint requests to Miklós S. Z. Kellermayer, Tel.: 36-72-536-271; Fax: 36-72-536-261; E-mail: miklos.kellermayer.jr@aok.pte.hu.

0006-3495/06/10/2665/13 $2.00

doi: 10.1529/biophysj.106.085456

Latham, NY) in a home-built spin processor. Two parafilm stripes, forming spacers, were positioned in parallel on the coverslip, and an 18 × 18-mm glass coverslip was added on top so that a flow-through microchamber suitable for TIRFM imaging was constructed. A 10-μl aliquot of HMM (100 μg/ml) diluted in assay buffer (AB, 25 mM imidazole-HCl, pH 7.4, 4 mM $MgCl_2$, 2 mM EGTA, 25 mM KCl, 1 mM dithiothreitol (DTT)) was first added to the chamber. Subsequently, the surface was blocked with bovine serum albumin (BSA, 0.5 mg/ml in AB). TRITC-phalloidin-labeled actin filaments (7-nM final concentration) were then added. To reduce photobleaching, the final buffer contained 100 mM β-mercaptoethanol and an oxygen-scavenger enzyme system (16). To access actin filaments with the AFM cantilever tip, the top coverslip was gently removed from the flow-through microchamber.

Cell culture

HeLa cells were a kind gift from the Immunology and Biotechnology Department, University of Pécs, Faculty of Medicine. Human pancreatic cancer cells (Panc-1) expressing K8 and K18 keratins were a kind gift from the Medical University of Ulm, Germany. Cells were maintained in Dulbecco's modified Eagle medium (DMEM) containing 10% fetal bovine serum, 2% L-glutamine, 1% penicillin-streptomycin at 37°C in a humidified 5% CO_2 atmosphere. For imaging, the cells were passed onto round coverslips (25-mm diameter, No. 1) and grown to subconfluence. Before experiments, Panc-1 cells were washed twice in serum-free DMEM and subsequently incubated for 18 h in serum-free DMEM.

Fluorescent labeling of cytoskeletal filaments

Washing and staining of samples were carried out in six-well plates. Cells were washed with phosphate-buffered saline solution (PBS, 10 mM K-phosphate, 140 mM NaCl), then permeabilized with Triton X-100 (0.1% in PBS) for 30 min at room temperature. Cells were fixed with paraformaldehyde (2% in PBS) for 15 min, washed with ethanolamine (10 mM in PBS) for 5 min, then rinsed with PBS. The actin-filament cytoskeleton was labeled with TRITC-phalloidin (200 nM in PBS complemented with 1% BSA) for 20 min at room temperature. Unbound TRITC-phalloidin was removed by washing with PBS. In the case of Panc-1 cells, keratin intermediate filaments were labeled with anti-pan-cytokeratin antibodies (KL1, Beckman-Coulter, Palo Alto, CA) for 30 min at room temperature, then the samples were labeled with fluorescein-isothiocyanate (FITC)-conjugated anti-mouse IgG antibodies. The round coverslips carrying the cells were mounted on a thin (2-mm) large-bore (23-mm) glass ring plate with silicon grease, so that the sample could be positioned on the microscope stage and accessed with AFM cantilever tip and objective lens at the same time. The cells were left covered with PBS complemented with 100 mM β-mercaptoethanol to reduce photobleaching.

Synchronized TIRF/AFM Imaging

Fluorescently labeled cells and molecules were visualized with a partly custom-built STIRF and AFM combination (Fig. 1). The objective-based TIRF microscope is built on an Olympus IX81 motorized epifluorescence microscope with a TIRF module (Olympus, Tokyo, Japan) and a 60×, 1.45 numerical aperture oil-immersion objective lens. Light from a green laser (YAG 532 nm, 50 mW, JDS Uniphase, Milpitas, CA) and a blue laser (488 nm, 15 mW, Novalux, Sunnyvale, CA) were joined with a long-pass dichroic mirror and coupled to the TIRF module via an optical fiber (Point Source, Hamble, UK). The angle of incidence was adjusted by positioning the free fiber end in the plane conjugate to the back focal plane of the objective lens.

The size of the illuminated field was adjusted with a field diaphragm conjugate with the sample plane. Emitted fluorescence was collected via a long-pass dichroic, emission filter, collector lens, internal reflection filter, and a confocal aperture (40 μm) and detected with an avalanche photodiode (APD, EG&G, Toronto, Canada). The signal was processed by either counting the photons with a digital access module (Asylum Research, Santa Barbara, CA) or by calculating intensity with a rate meter (Supertech, Pécs, Hungary). The sample was positioned on a special, double XY microscope stage, which is part of the AFM system (MFP-3D, Asylum Research) (Fig. 1, *upper inset*). The lower, mechanical stage permits the movement of the AFM head (together with the upper, sample stage) relative to the optical axis. The upper, sample stage is a closed-loop XY-piezo stage. To obtain spatially synchronized AFM and TIRFM images, the cantilever tip was aligned with the optical axis by manually positioning the AFM head with the lower stage under video control. Silicon nitride (Si_3N_4) cantilevers (Olympus) were used for scanning either in air (AC160TS, resonance frequency ~300 kHz) or in liquid (BioLever, lever B, Au-coated on both sides, resonance frequency ~35 kHz). Images (512 × 512 pixels or 1024 × 1024 pixels) were collected at a typical scanning frequency of 1 Hz. To obtain temporal synchrony, the fluorescence and AFM signals were simultaneously recorded and stored in parallel data sets (''waves'', IgorPro, Wavemetrics, Lake Oswego, OR).

Focused TIRF microscopy

To reduce the size of the illuminated area to the diffraction limit and to increase excitation intensity, we used a focused TIRF arrangement (Fig. 1, *lower inset*). This arrangement is analogous to a confocal microscope in which a stationary, but tilted (and focused) laser beam is used for illumination. The instrumental arrangement was identical to that of wide-field TIRFM with one exception: we used a fiber optic cable with a collimator to couple the laser beam into the TIRF unit of the microscope. Thus, a collimated beam entered the back aperture of the objective, in contrast to the focused beam used in wide-field TIRFM. Tilting of the illuminating beam was accomplished by positioning the fiber-coupling assembly in the conjugate plane of the objective back aperture. The relatively large diameter (~2 mm) of the beam entering the objective back aperture resulted in a wide range of incident angles at the sample plane (Fig. 1, *lower inset*). Only in the case of the largest incident angles did we obtain total internal reflection. Rays arriving at the sample at angles smaller than the critical angle became refracted. Thus, the excitation beam was partitioned into a reflected and a refracted portion. In our experiments we positioned the excitation laser beam in such a way that the rays passing through the sample were tilted away from the cantilever, but the beam was entirely within the back aperture.

Mechanical manipulation of fluorescently labeled, surface-attached soft samples

Mechanical manipulation of TRITC-labeled, cultured HeLa cells or individual, HMM-attached actin filaments was carried out by first coaligning, to within ~1 μm, the AFM cantilever (Olympus AC160TS) with the optical axis and scanning an initial TIRF microscopic image. Subsequently a user-defined nanolithographic pattern was drawn into the surface with a typical pressing force of ~1 nN, using the MicroAngelo program routines of the AFM driving software (Asylum Research). Finally, a second scanning TIRFM image was obtained.

Single-molecule force spectroscopy of fluorescently labeled titin

TMRIA-labeled titin molecules were first attached to the AFM cantilever (Olympus BioLever, lever B) by pipetting an aliquot (5 μl) of sample (0.05 mg/ml) onto the cantilever tip and incubating at room temperature for 10 min. Unbound molecules were removed by successive washes with buffer (AB with 200 mM KCl). The titin-coated cantilever was pressed in the evanescent field of wide-field TIRFM and brought near a cleaned microscope coverslip. The cantilever tip was coaligned with the optical axis by moving the tip in the XY direction and seeking the maximum in the APD signal. The cantilever tip was than pressed onto the coverslip surface with

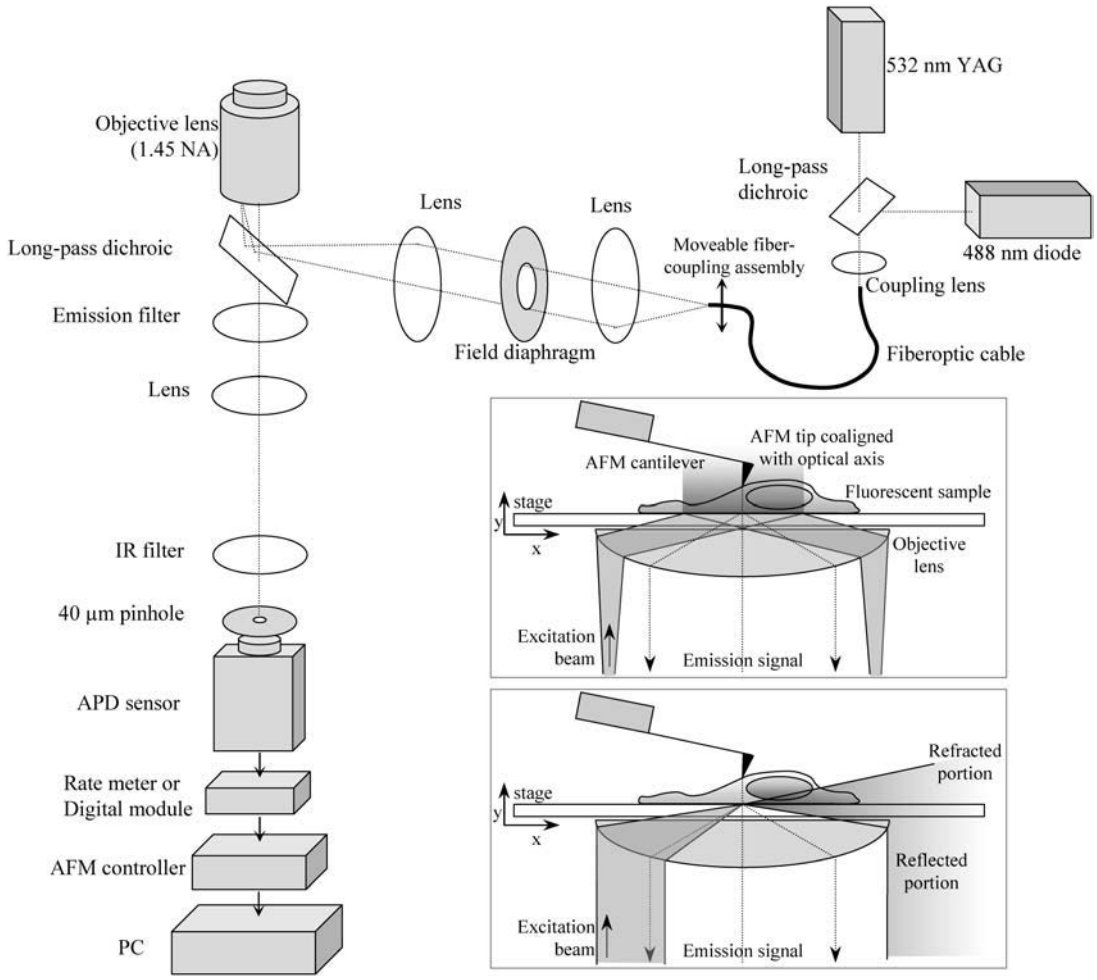

FIGURE 1 Schematics of the epifluorescence optical path of the synchronized TIRF/AFM instrument. (*Upper inset*) Schematics of wide-field TIRFM combined with AFM. (*Lower inset*) Schematics of confocal, partial TIRFM (focused TIRFM) combined with AFM.

constant rate (typical rates 500 nm/s). Cantilever displacement and deflection signals were collected. Cantilever stiffness was calibrated with the thermal method (17–19). Typical cantilever stiffness was ~30 pN/nm.

Data analysis and processing

Image processing was carried out using the built-in routines of the MFP3D software. Three-dimensional (3D) surface rendering was done with the Argyle toolbox of the MFP3D software. For calculations and statistical analyses we used IgorPro (v. 5.0) and KaleidaGraph (v. 4.0) software packages. Whenever necessary, nonlinear force curves were fitted with the worm-like chain model of entropic elasticity (20).

RESULTS

Spatially and temporally synchronized TIRFM and AFM

A spatially and temporally synchronized TIRFM and AFM instrument was assembled for the purpose of simultaneous acquisition of topography/mechanics and fluorescence information on cells and biomolecules. We hereby abbreviate this combined, multi-faceted instrument as STIRF-AFM. The schematics of the instrument layout are shown in Fig. 1. The instrumentation was assembled from commercially available and custom-built items. A stage-scanning AFM instrument was combined with an objective-based TIRF microscope. For measuring fluorescence emission, a photon-counting module was attached to the bottom port of the epifluorescence microscope. Temporal synchronization between AFM and TIRFM was achieved by simultaneous acquisition of the cantilever-related (deflection, height, amplitude, and phase) and fluorescence (photon count or fluorescence intensity) data. Spatial synchronization was established by positioning the cantilever onto the optical axis (Fig. 1 *inset*). As long as the cantilever remained coaligned with the optical axis, spatial synchronization was maintained, typically within the diffraction limit. Further details of the instrumental arrangement are described in Materials and Methods. The STIRF-AFM instrument was tested and validated on various biomolecular and cellular systems such as cultured monolayer cells, actomyosin, and titin.

Stage-scanning, evanescent field excitation confocal microscopy

For fluorescence imaging in synchrony with AFM data acquisition, we first developed a stage-scanning, evanescent field excitation confocal microscope (Fig. 1). In this arrangement the fluorescence image was obtained by scanning the sample in the evanescent field and collecting photon count or intensity data at each point of the scan. The size of the illuminated area was limited by using a field diaphragm positioned in the excitation beam path in a focal plane conjugate with the sample. To maintain high spatial resolution, a pinhole (40 μm) was positioned in front of the photon counting module. The signal from the photon counting module was either used directly as number of photons per image pixel or converted to intensity by using a rate meter. The pixel size, set by the ratio of the scan size ($\sim$5–70 μm for the images herein) and image resolution (typically 512 $\times$ 512), varied between $\sim$10–140 nm. In terms of image quality we found no significant difference between the two acquisition methods.

We tested the stage-scanning, evanescent field excitation confocal microscope on samples of surface-attached actin filaments and HeLa cells in which the actin cytoskeleton was labeled with TRITC-phalloidin (Fig. 2). The fluorescence image of TRITC-labeled actin filaments attached in rigor state to a HMM-coated surface is shown in Fig. 2 *a*. The image is essentially indistinguishable from that recorded with a microchannel-plate-intensified charge-coupled device (CCD) camera (data not shown). The half-maximum width of the Gaussian intensity profile across the actin-filament image (Fig. 2 *b*) was 394 nm, which is comparable with the optical resolution for this emission wavelength (580 nm). We found that the root mean-square (RMS) variation of the fluorescence intensity along an actin filament in the evanescent field was 60 in contrast to that of the background, which was 17 (Fig. 2 *c*). The large spatial variation of emission intensity along the actin filament might be due to a variation of the filament position in the evanescent field. The scanning TIRF image of TRITC-phalloidin-labeled HeLa cells is shown in Fig. 2 *d*. Bundles of actin filaments running parallel to the microscope coverslip surface can be clearly visualized.

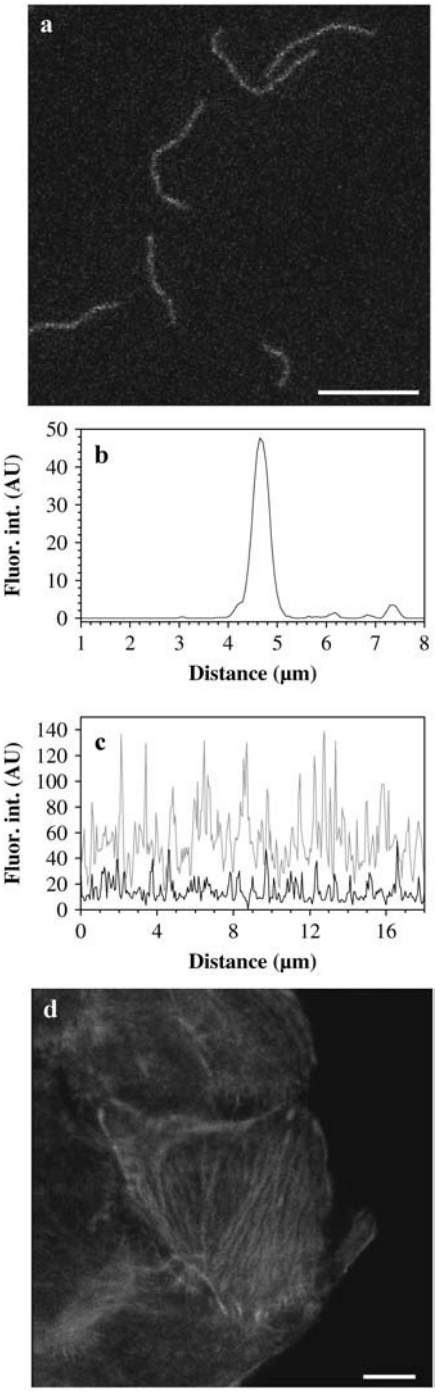

FIGURE 2 (*a*) Image of individual actin filaments bound to an HMM-coated surface acquired with scanning wide-field TIRFM. Scale bar, 10 μm. (*b*) Intensity profile across an actin filament. (*c*). Intensity profile along the contour of an actin filament (*gray*) and along an arbitrary line in the background (*black*). (*d*) Scanning wide-field TIRFM image of HeLa cells labeled with TRITC-phalloidin. The cells were fixed with paraformaldehyde, then washed and imaged in PBS. Scale bar, 10 μm.

Imaging with synchronized TIRFM and AFM

The synchronized TIRFM and AFM (STIRF-AFM) instrument was tested and validated by imaging fluorescently labeled monolayer cell cultures and surface-adsorbed titin molecules. The STIRF-AFM image of TRITC-phalloidin-labeled, dried HeLa cells is shown in Fig. 3. The main cellular components and filaments of the detergent-resistant cytoskeleton can be clearly visualized on the topography images (AFM height, amplitude, and phase contrast). The scanning TIRFM image revealed that the actin-rich structures are localized at the cell's edge and the perinuclear

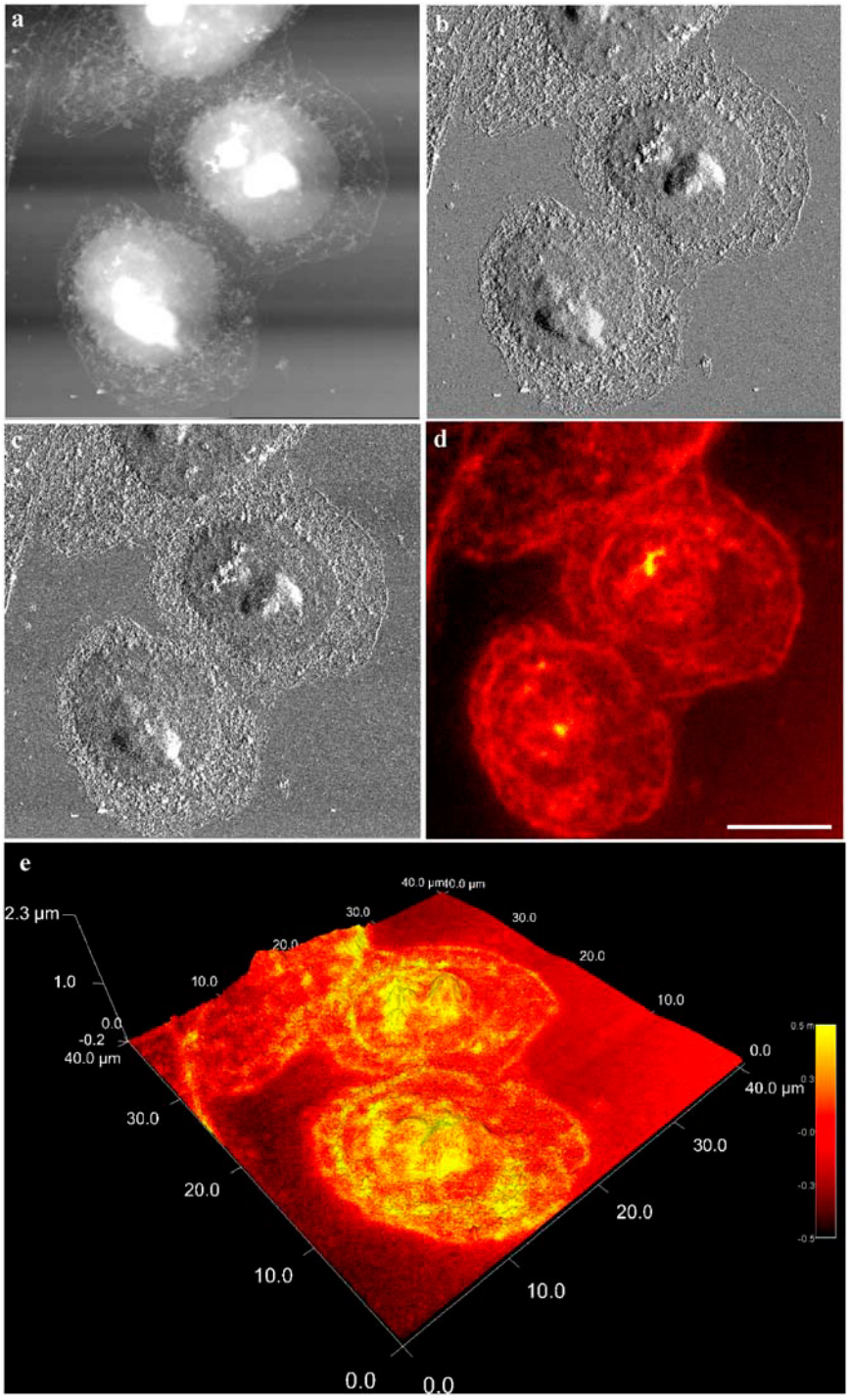

FIGURE 3 Image of cultured HeLa cells acquired with synchronized TIRF-AFM. (*a*). Height contrast. (*b*) Amplitude (error) contrast. (*c*) Phase contrast. (*d*) TIRF image. Scale bar, 10 μm. (*e*) 3D surface plot of height image colored with fluorescence data. Color bar shows rate meter readings in millivolts, which corresponds to fluorescence intensity. The cells were fixed, labeled with TRITC-phalloidin, washed with PBS and water, then dried with a stream of high-purity N_2 gas.

region. Furthermore, there is considerable fluorescence in the nucleolar region. A 3D-rendered STIRF-AFM image is shown in Fig. 3 *e*. In this image, the AFM height image is shown in 3D, and the color corresponds to fluorescence intensity. The image shows that the maximal height of the cells was only a couple hundred nanometers, which is most likely due to a structural collapse caused by dehydration.

Magnified STIRF-AFM images of the edge of a cultured HeLa cell are shown in Fig. 4. Filamentous components of the detergent-resistant cytoskeleton can be identified. Thick bundles of filaments are actin-containing stress fibers, as evidenced by the simultaneously obtained scanning TIRFM images (Fig. 4, *e* and *f*). The lateral offset of ~300 nm apparent between the AFM (Fig. 4 *d*) and the TIRFM (Fig. 4 *f*) images also indicates that a residual misalignment is present between the cantilever tip and the optical axis.

For molecular imaging with STIRF-AFM, we scanned a glass surface coated with titin labeled with Oregon Green

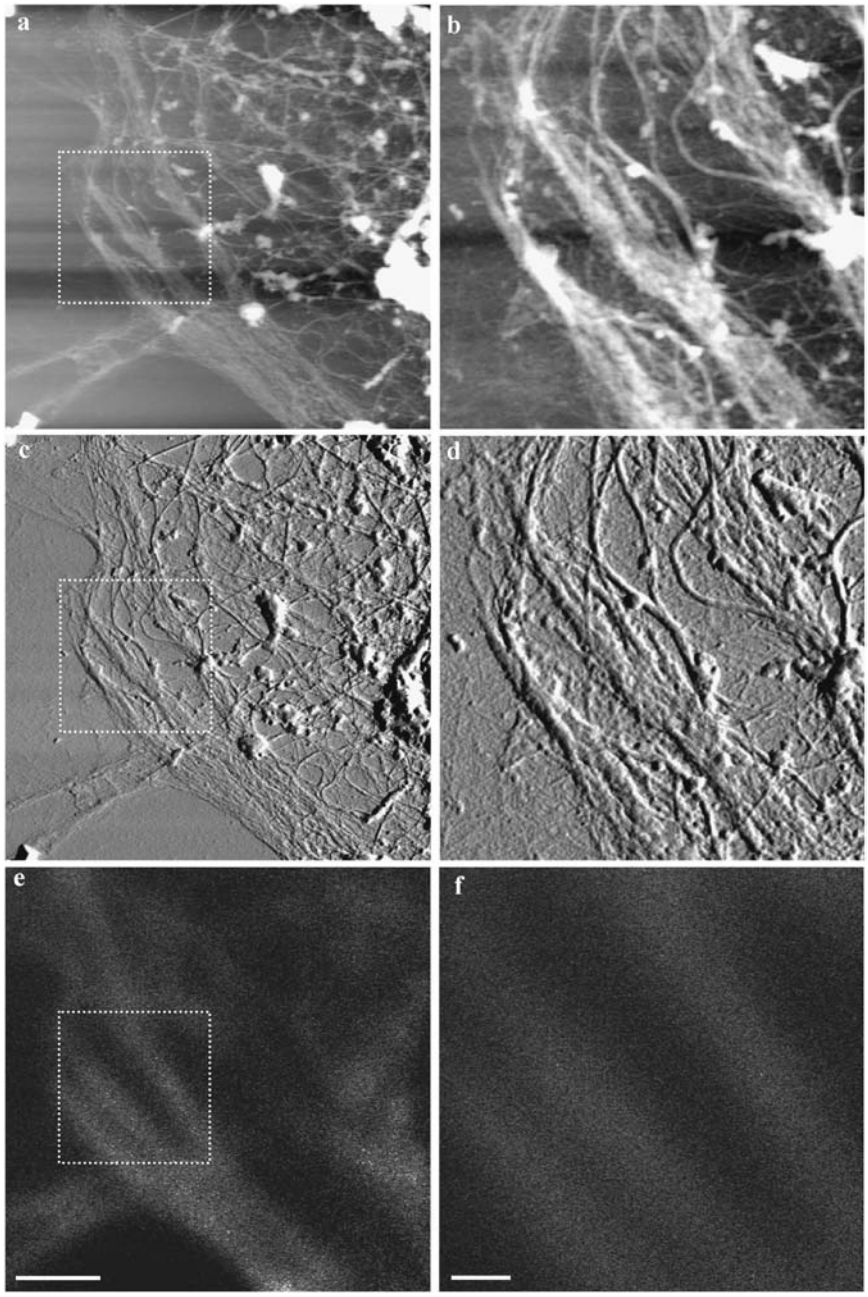

FIGURE 4 Images of subcortical actin-containing filamentous structures in cultured HeLa cells acquired with synchronized TIRF-AFM. (*a*) Low-magnification height contrast image. (*b*) High-magnification height contrast image. (*c*) Low-magnification amplitude contrast image. (*d*) High-magnification height contrast image. (*e*) Low-magnification scanning wide-field TIRFM image. Scale bar, 2 μm. (*f*) High-magnification scanning wide-field TIRFM image. Scale bar, 500 nm.

488-maleimide (Fig. 5). Molecular topography (Fig. 5 *a*), fluorescence (Fig. 5 *b*), and their 3D rendering (Fig. 5 *d*) are shown. The compact titin particles observed in Fig. 5 *a* are most likely contracted titin oligomers. For comparison, the same titin sample was adsorbed to mica and imaged in air (Fig. 5 *c*). Head-to-head titin oligomers (21) are observed.

STIRF-AFM images of cultured pancreas carcinoma cells (Panc-1) labeled with TRITC phalloidin and anti-cytokeratin antibody and FITC-conjugated secondary antibody are shown in Fig. 6. Fluorescence was acquired simultaneously with AFM topography, but scanning for the different fluorescence emissions was carried out sequentially. As evidenced by the STIRF-AFM images, most of the actin fluorescence is located in the periphery of the cell, including filopodia, and considerable fluorescence is observed in the cell nucleus. Intermediate filament fluorescence is most intensive in the perinuclear region.

Focused STIRF-AFM

To increase local excitation intensity and to reduce the size of the illuminated area, we combined AFM with focused TIRF microscopy (Fig. 7). In this experimental arrangement a focused and tilted laser beam was used to excite the sample

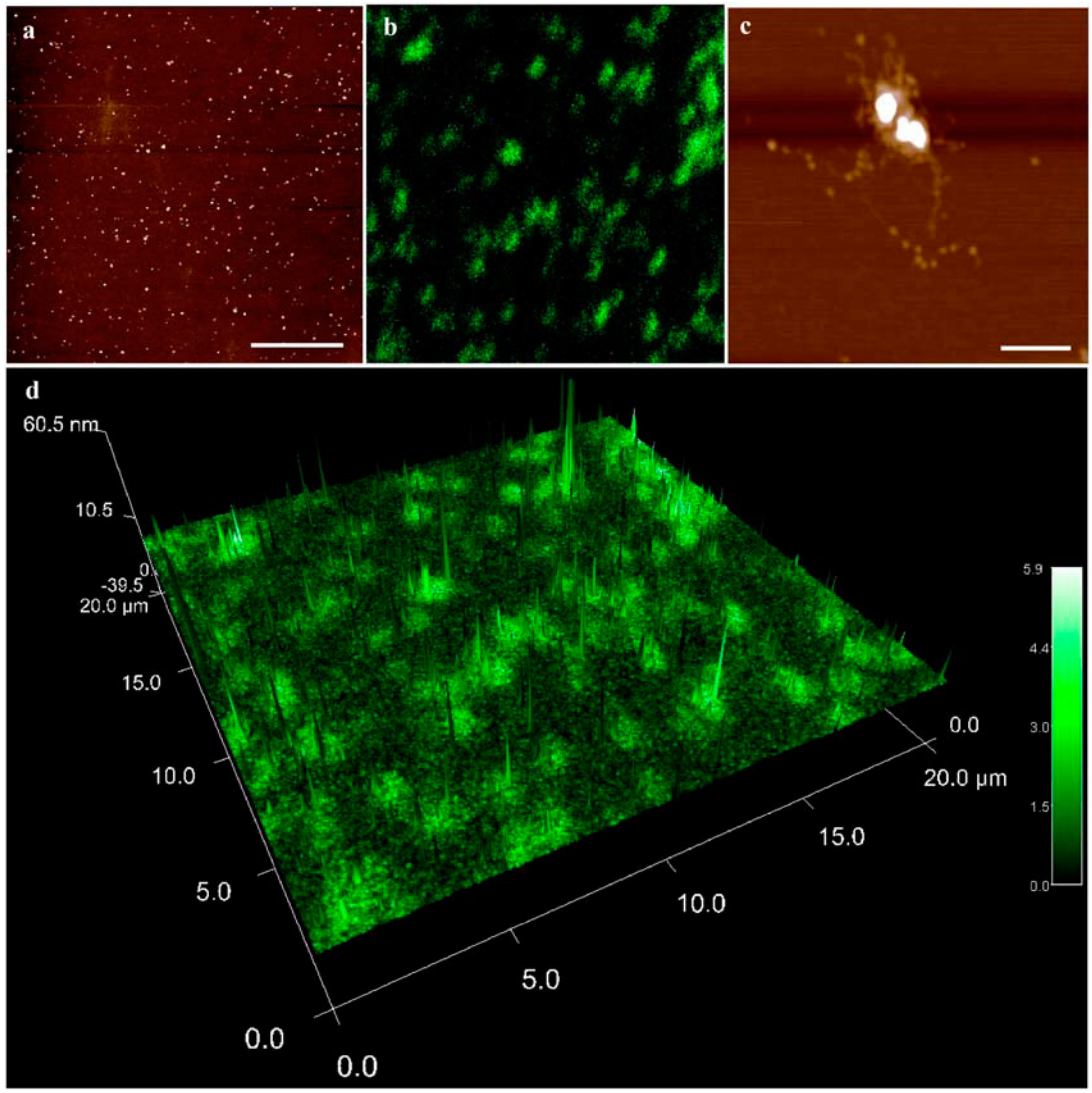

FIGURE 5 Synchronized TIRF-AFM image of Oregon-Green-488-labeled titin molecules. (*a*) Height contrast AFM image obtained by scanning in liquid with Olympus BioLever in AC mode. Scale bar, 5 μm. (*b*) Scanning TIRFM image obtained simultaneously with *a*. (*c*) AFM image of a titin oligomer adsorbed to mica obtained by scanning in air with Olympus AC160 cantilever. Scale bar, 200 nm. (*d*) 3D surface plot of *a* colored with the fluorescence information (*b*).

at the location of the AFM cantilever tip. A large spatial power density was achieved that resulted in bright fluorescence images (Fig. 7, *c* and *e*). Focused STIRF-AFM images of a cultured, TRITC-phalloidin-labeled and dried HeLa cell are shown in Fig. 7, *a–c*. Because of spatial synchrony, local fluorescence intensity can be compared with and mapped onto the surface topography. Such a correlated topographical height and fluorescence function is shown in Fig. 7 *d*.

Although the spatial power density was very high in focused STIRF-AFM, photobleaching became reduced in comparison to wide-field TIRFM because of the limited time that the focused beam stayed on the sample. We tested photobleaching induced by focused TIRFM by scanning the same region of interest over and over several times (Fig. 7, *e* and *f*). Even after four scans, individual actin-filament bundles were clearly visualized. In comparison, image quality became poor only after two scans with wide-field TIRFM (data not shown).

Mechanical manipulation with STIRF-AFM

Observations on the mechanical manipulation of cells and molecules with STIRF-AFM are shown in Fig. 8. In the first set of experiments we used STIRF-AFM to ablate parts of surface-attached cells and actin filaments (Fig. 8, *a* and *b*). Because of spatial synchrony, areas to be mechanically manipulated can be defined and targeted with high (submicron) precision. As evidenced by the images, targeted parts of the surface-attached HeLa cells and actin filaments were successfully removed with the technique.

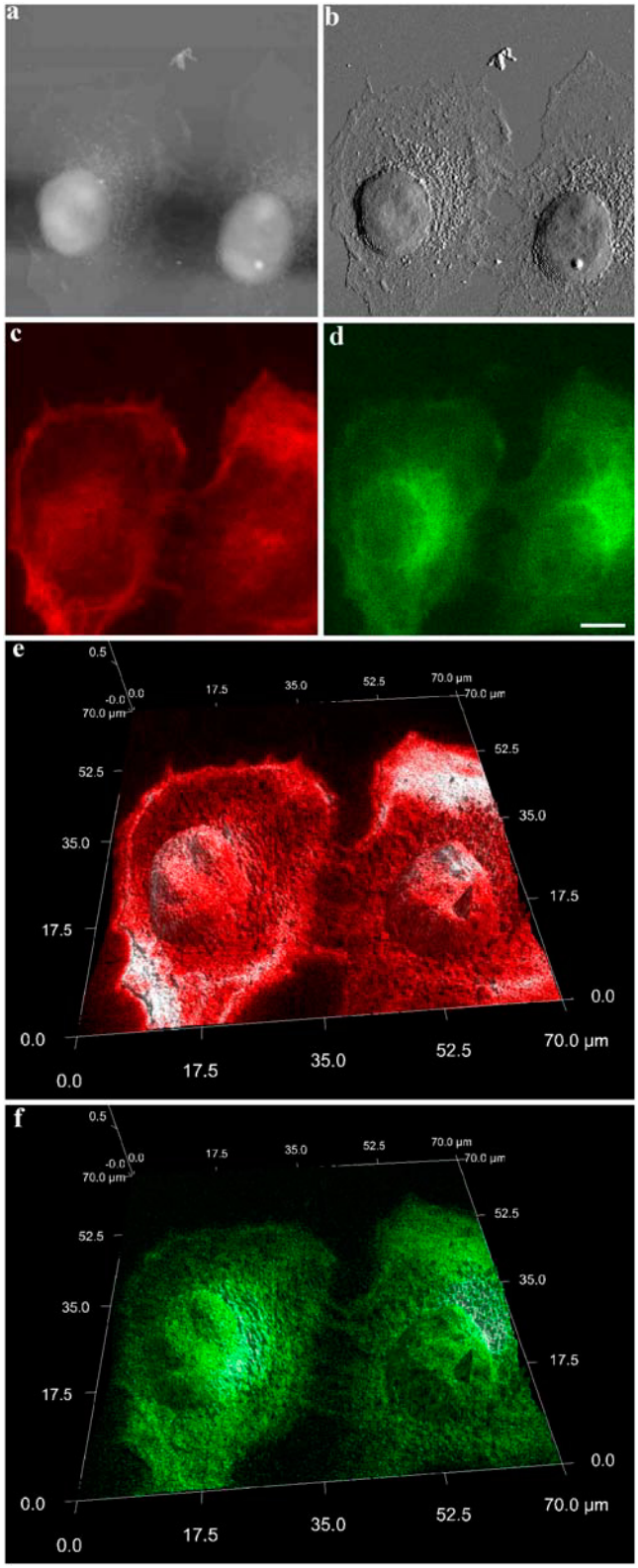

FIGURE 6 Dual-color synchronized TIRF-AFM images of pancreas carcinoma cells labeled with TRITC-phalloidin and anti-cytokeratin antibodies. Red and green fluorescence images were acquired in sequential scans. (*a*) Height contrast image. (*b*) Amplitude contrast image. (*c*) Red fluorescence image, corresponding to F-actin distribution. (*d*) Green fluorescence image, corresponding to cytokeratin distribution. Scale bar, 10 μm. (*e*) 3D surface plot colored with the red fluorescence information. (*f*) 3D surface plot colored with the green fluorescence information.

To further test and validate the STIRF-AFM method, we mechanically manipulated TMRIA-labeled titin molecules preadsorbed either to the coverslip surface (Fig. 8 *c*) or to the AFM cantilever tip (Fig. 8 *d*). In the case of surface-adsorbed titin, a scanning TIRFM image was first prepared based on which a molecule was selected and coaligned with the optical axis. Subsequently, the AFM cantilever tip was pressed against the molecule, then pulled away with a constant, preadjusted velocity. If the titin molecule became attached to the AFM tip, then it became stretched by the procedure (Fig. 8 *c*, *inset*). The elastic response of the titin molecules was followed by measuring force as a function of extension. Simultaneously acquired force and fluorescence data of TMRIA-titin as a function of extension are shown in Fig. 8 *c*, *i–iii*. Sawtooth force transitions superimposed onto nonlinear force curves, typical for titin (21,22), were observed. In the fluorescence traces sometimes we observed abrupt increases in fluorescence intensity, indicating that a structural change probably occurred in the part of the titin molecule that remained in the evanescent field. In the case of tip-adsorbed titin, molecules were stretched by lowering the tip onto the coverslip surface, then pulling the tip away with a given stretch velocity (Fig. 8 *d*, *inset*).

If titin molecules became attached to the coverslip surface, then these molecules became stretched by the procedure. In these experiments the fluorescence traces were dominated by a single-exponential decay that most likely corresponds to the movement of the fluorescent tip in the exponentially decaying evanescent field (Fig. 8 *d*). In support of this notion, the movement of uncoated Si_3N_4 tip, which we found to be brightly fluorescent at the 532-nm excitation wavelength, also resulted in exponentially decaying fluorescence intensity (Fig. 8 *e*). By decreasing the angle of incidence of the excitation laser beam, the depth of the evanescent field increased as previously observed (9). In the case of tip-adsorbed titin, we also observed sudden changes in fluorescence intensity (Fig. 8 *d*, *asterisk*).

DISCUSSION

A combined stage-scanning TIRF microscope and AFM was developed in this work. With the instrument, spatially and temporally synchronized fluorescence and topography imaging became feasible. We hereby abbreviate the name of the method ''STIRF-AFM''.

There are numerous motivations for combining AFM with fluorescence. AFM provides high-resolution topography and mechanics (viscoelasticity) information of the examined specimen (1). Furthermore, it is possible to directly manipulate the sample mechanically (22,23), a method that has evolved into single-molecule force spectroscopy (2). Various

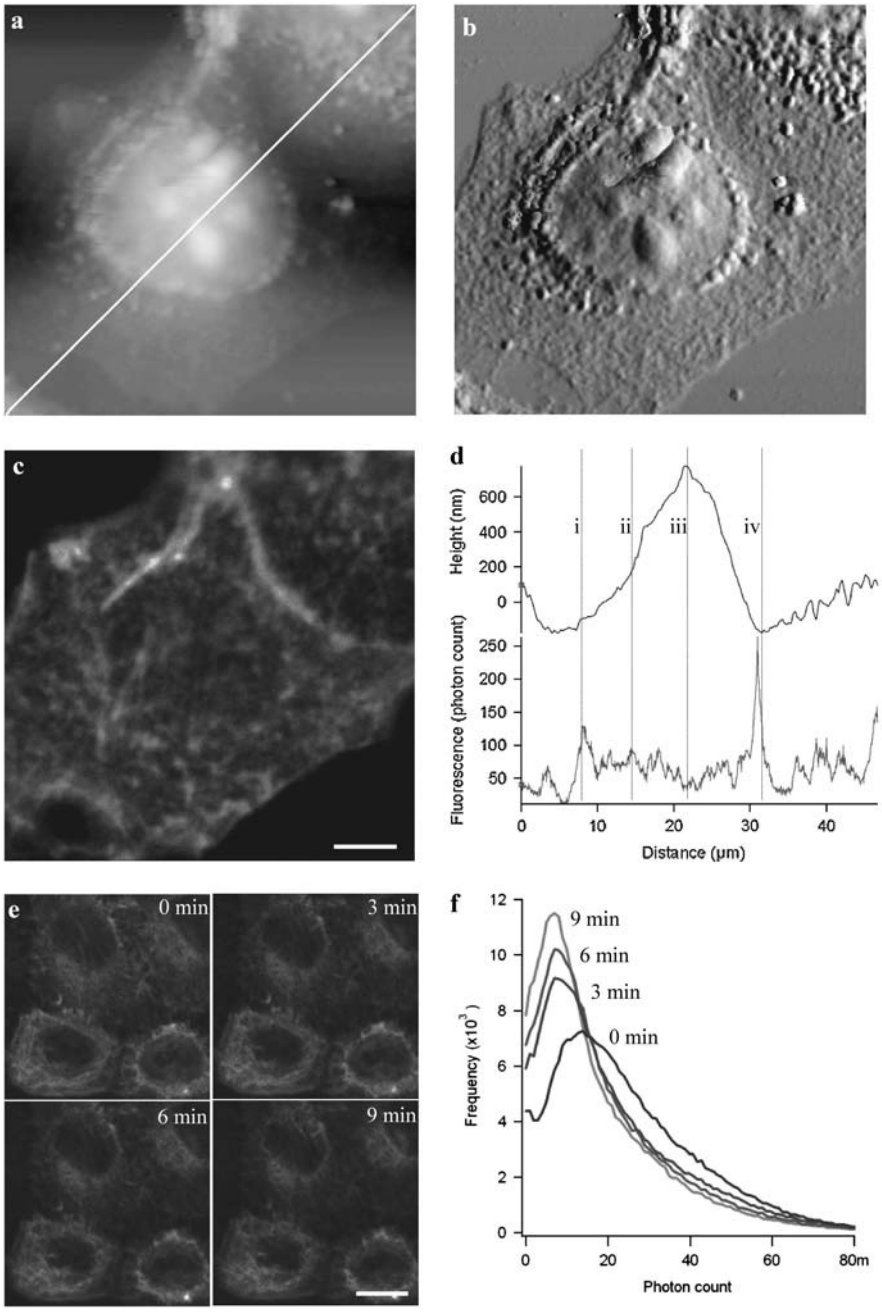

FIGURE 7 Imaging cultured HeLa cells with synchronized focused TIRF-AFM. (*a*) Height contrast image. White diagonal line marks the region from where synchronized data were plotted. (*b*) Amplitude contrast image. (*c*) Focused STIRF-AFM image. Scale bar, 5 μm. (*d*) Spatially correlated height and fluorescence intensity. Subcortical actin filaments (*i*), edge of cell nucleus (*ii*), nucleolus (*iii*), and subcortical actin filaments at the other edge of the cell (*iv*) are indicated. (*e*) Testing of photobleaching in sequential scans with focused STIRF-AFM. The acquisition of each scan required 3 min. (*f*) Color density histograms of the focused STIRF-AFM images.

modalities of fluorescence (intensity, polarization, anisotropy, and lifetime) provide dynamic and structural information related to the local physical-chemistry of the specimen (3,24,25). In certain fluorescence modes (fluorescence resonance energy transfer, FRET) structural information of very high resolution may be obtained (26,27).

There have been many attempts to combine AFM and fluorescence imaging (4–6,8,9,28,29). Due to the vast differences in acquisition rates and modes of imaging, the acquisition of AFM and fluorescence has usually been sequential. A direct correlation of the fluorescence and AFM data in these methods is difficult, and typically they are segregated in separate data sets. To establish fully synchronized AFM and fluorescence imaging, we carried out sample scanning and coaligned the optical and mechanical axes. In this imaging mode, at each point of the sample scan the mechanical (cantilever deflection) and fluorescence (emitted photons) information were recorded simultaneously.

As a first step in establishing synchronized fluorescence and AFM imaging, we developed a sample-scanning fluorescence imaging method. Ideally, fluorescence excitation should be spatially limited to the part of the sample being examined with the AFM cantilever tip, but the excitation beam should not interfere with the cantilever itself. We

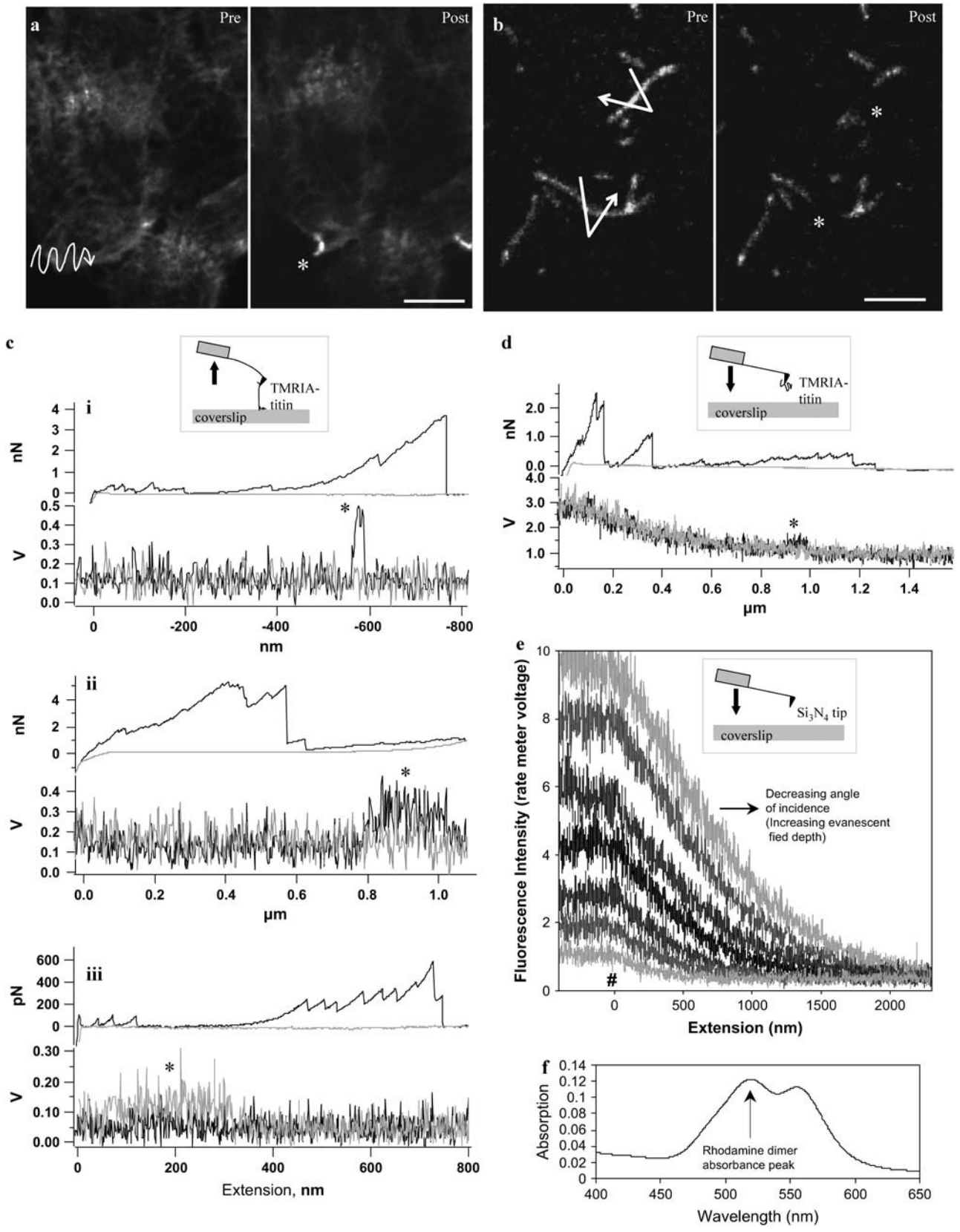

FIGURE 8 Mechanical manipulation of cells and molecules with synchronized TIRF/AFM. (*a*) Ablation of a section of a cultured HeLa cell labeled with TRITC-phalloidin. The image labeled ''Pre'' shows the conditions before mechanical manipulation. White line indicates with arrow the lithographic path traveled by the cantilever tip. The image labeled ''Post'' shows the effect of mechanical manipulation. The region marked with a star is the section of the cell

experimented with two excitation geometries, each of which partly fulfills the ideal requirements. We used TIRF, in which the depth of the evanescent field that excites the fluorophores is on the order of a couple hundred nanometers (7), and therefore interference with AFM imaging is unlikely since the cantilever tip is typically $>10\times$ longer than this. First, we used wide-field, objective-based TIRF microscopy (Figs. 1, *upper inset*, 2–6, and 8, *c–e*), in which an illuminated area of the sample was limited with a field diaphragm to ~ 5 μm. Second, we used a focused TIRF arrangement, in which the sample was illuminated with a focused and tilted laser beam (Figs. 7 and 8, *a* and *b*).

Focused TIRFM in an arrangement resembling dark-field illumination was recently used to excite attoliter volumes of fluorescently labeled sample (30). In our arrangement of focused TIRFM, only part of the participating rays is totally reflected, because they arrive at the sample at a wide range of incident angles. Nevertheless, the refracted rays do not interfere with the cantilever either. We found that very high signal/noise ratio and low photobleaching are obtained with scanning, focused TIRFM. In the case of stationary samples used in single-molecule force spectroscopy (Fig. 8, *c–e*), however, wide-field TIRFM may be better suited. The advantages of focused TIRFM over the wide-field arrangement are 1), high excitation intensity, 2), low photobleaching, and 3), improved spatial resolution (alleviation of the need for a confocal pinhole). The main disadvantage of focused TIRFM is its cumbersome alignment: the excitation focal point must be coaligned with the detection volume for an in-focus specimen by tilting the laser beam in the conjugate focal plane of the objective back aperture.

The spatial resolution reached with scanning TIRFM is on the order of the diffraction limit (Fig. 2). In fact, images obtained on single actin filaments with scanning TIRFM are indistinguishable from those obtained with microchannel-plate-intensified CCD cameras. Furthermore, because of the narrow excitation field, local variations in fluorescence intensity, possibly related to filament position relative to the surface, may be detected (Fig. 2 *c*). The time resolution of scanning TIRFM imaging matches that of AFM scanning. Therefore, obtaining a TIRFM image takes several minutes. Because of the low image acquisition rate and the narrow excitation field, focusing is often difficult. Refocusing during scanning requires precautions because movement of the oil-immersion objective, which is in viscous coupling with the sample, causes noise in simultaneous AFM scanning. We are currently developing means to establish automatic focusing that addresses the problem of the additional mechanical noise. In contrast to the low image acquisition time resolution, when fluorescence is measured at a single, user-defined point, acquisition rates up to 100 kHz (limited by analog-to-digital conversion rate) may be reached.

We successfully combined scanning TIRFM imaging with AFM (Figs. 3–7). Complete temporal synchrony was achieved because of simultaneous acquisition of the photon count and AFM data. Spatial synchrony was obtained by positioning the cantilever tip onto the optical axis. That is, the cantilever tip was positioned on the location sensed by the photon-counting module. In this work, we established spatial synchronization by positioning, under video control and using stage micrometers, the cantilever tip to an empirically determined location before the scanning experiment. Most often we were able to achieve spatial synchrony within the diffraction limit (see Fig. 5). At higher magnifications, however, residual discrepancies between spatial correspondence became evident (Fig. 4). Furthermore, spatial synchronization is sensitive to drift, and constant readjustments, using closed-loop piezo translators and fiducial image coordinates, may be necessary. Using STIRF-AFM we obtained spatially and temporally synchronized images of monolayer cells in culture.

To validate the method, in this work we used fixed and dried cells, which are easier to scan with AFM. Microfilament (Figs. 3, 4, and 6) and intermediate filament (Fig. 6) components of the cytoskeleton could be visualized and localized with the method and matched with surface topography elements. Importantly, because of synchronized AFM and optical imaging, problems associated with independent nonlinearities of the two imaging methods are alleviated. We successfully employed STIRF-AFM to image surface-adsorbed, fluorescently labeled titin molecules (Fig. 5). Optical resolution issues related to the diffraction limit become particularly visible with our imaging method, because single fluorescent spots often contained two or more titin

Figure 8 (Continued).
that has been removed. Scale bar, 10 μm. (*b*) Cutting actin filaments using nanolithographic methods. The image labeled ''Pre'' shows the conditions before the mechanical manipulation. White lines with arrows indicate the lithographic paths traveled by the cantilever tip. The image labeled ''Post'' shows the effect of the mechanical manipulation. The regions marked with a star are areas from which a segment of the respective actin filaments were removed. Scale bar, 5 μm. (*c*) Mechanical manipulation of TMRIA-labeled titin preadsorbed to the cantilever tip (Olympus BioLever). (*Framed inset*) Schematics of the experimental arrangement. (*c*) (*i–iii*) Examples of force curves. Black line is data obtained during stretch; gray line is data obtained during relaxation. Sudden changes in fluorescence intensity are marked with asterisk. (*d*) Mechanical manipulation of TMRIA-labeled titin preadsorbed to the glass coverslip surface. The cantilever was Olympus BioLever. (*Framed inset*) Schematics of the experimental arrangement. Black line is data obtained during stretch, gray line is data obtained during relaxation. Sudden change in fluorescence intensity, observed in the stretch data, is marked with asterisk. (*e*) Fluorescence intensity as a function of tip-surface distance and evanescent field depth. (*Framed inset*) Schematics of the experimental arrangement. Silicon-nitride cantilever Au-coated on backside was used (Veeco Microlever). The number sign (#) indicates the location of tip-surface engagement. (*f*) Absorption spectrum of the TMRIA-labeled titin sample used in the experiments.

molecules as revealed with the AFM scanning (Fig. 5 *a*). STIRF-AFM may aid in identifying the exact number of molecules behind a single spot in the fluorescence image.

AFM tip fluorescence may interfere with obtaining high-quality fluorescence images by reducing signal/noise ratio. Tip fluorescence emission depends on the cantilever type, excitation wavelength, and excitation intensity. We found that uncoated silicon nitride tips fluoresce when excited with 532 nm, but emission intensity is significantly reduced at 488-nm excitation. Gold coating on the tip surface significantly reduced tip fluorescence, probably because much of the excitation intensity was reflected by the tip.

A special application of STIRF-AFM is the mechanical manipulation of fluorescently labeled cellular and biomolecular samples (Fig. 8). Because of spatial synchrony, it is possible to first image the specimen with scanning TIRFM, then manipulate the sample at user-defined locations with AFM using nanolithography protocols, and finally reimage the sample with TIRFM to detect the evoked changes. We have successfully applied this method to ablate parts of cells and individual actin filaments (Fig. 8, *a* and *b*). A particularly interesting application of STIRF-AFM is in the exploration of mechanically driven structural changes in biomolecules. Currently very little is known about the details of structural changes evoked in single molecules by mechanical manipulation. Structural knowledge is inferred from particular aspects of the mechanical data (e.g., contour length calculated from fitting with polymer models) compared with independent structural data (e.g., contour length calculated from protein sequence) (22,31,32). A simultaneous but independent method that provides structural information may reveal the details of intramolecular changes evoked by mechanical perturbation. In the TMRIA-labeled titin-molecule strand stretched with AFM we sometimes observed sudden increases of fluorescence intensity (Fig. 8, *c* and *d*).

These bursts of fluorescence intensity were seen both during mechanical stretch and relaxation. We have previously shown that the fluorescence of TMRIA-labeled titin is quenched in the native state of the protein due to the formation of rhodamine dimers (14). Indeed, the 518-nm peak in the absorption spectrum of TMRIA-labeled titin used here (Fig. 8, *f*) revealed the presence of rhodamine dimers. Fluorescence intensity increases upon the addition of chemical denaturants to TMRIA-labeled titin (14). Possibly, the mechanical extension of titin and the concomitant unfolding of the molecule resulted in the dissociation of rhodamine dimers and hence in the increase of fluorescence intensity observed here. So far we have not been able to correlate the observed fluorescence changes with particular mechanical events such as the sawtooth-shaped force transitions. Furthermore, the detected fluorescence changes originate from parts of the titin molecule that remain in the evanescent field during the mechanical manipulation. It is also possible that sudden changes in the concentration of fluorophores within the excitation volume, caused by relaxation and contraction of the titin molecule, may also contribute to the observed fluorescence changes. Further work will help to sort out the exact mechanisms of our findings.

Further applications, widespread use, and future development of the STIRF-AFM instrument will probably depend on the ease of assembly and use, the costs involved, and the possibility of combination with other novel microscopic techniques (e.g., single-molecule polarization methods (33), FIONA (34)). The costs involved in constructing the instrument herein, in addition to the AFM and the light microscope, are related to lasers, coupling optical fibers, APD detector, and an intensified CCD camera for alignment purposes (altogether ~$30,000). Although setting the instrument up is relatively easy, frequent realignments are necessary to achieve spatial synchrony and high-quality images. Coalignment and autofocus algorithms, currently under development, may aid in improving the ease of use. Finally, the use of high-speed, high-resolution cameras instead of APD may expand the applicability of STIRF-AFM to novel fluorescence imaging methodologies.

In sum, a synchronized TIRF and AFM was developed and tested. The instrument, which we named STIRF-AFM, allows the visualization of surface topography and fluorescence of suitable cellular and biomolecular samples simultaneously. Furthermore, STIRF-AFM makes it possible to follow the fluorescence of mechanically manipulated molecules with high time resolution. Conceivably, STIRF-AFM may contribute to resolve the details of structural changes that occur in biological molecules upon mechanical manipulation.

This work was supported by grants from the Hungarian Science Foundation (OTKA T037935, T049591), Hungarian Ministry of Education (BIO-110/2002), Hungarian Ministry of Health (ETT-440/2003), the South Trans-Danubian Cooperative Research Center, and the Howard Hughes Medical Institute to M.S.Z.K. (International Research Scholarship).

REFERENCES

1. Binnig, G., C. F. Quate, and C. Gerber. 1986. Atomic force microscope. *Phys. Rev. Lett.* 56:930–933.
2. Rief, M., and H. Grubmuller. 2002. Force spectroscopy of single biomolecules. *ChemPhysChem.* 3:255–261.
3. Kellermayer, M. S. Z. 2005. Visualizing and manipulating individual protein molecules. *Physiol. Meas.* 26:R119–R153.
4. Gorelik, J., A. Shevchuk, M. Ramalho, M. Elliott, C. Lei, C. F. Higgins, M. J. Lab, D. Klenerman, N. Krauzewicz, and Y. Korchev. 2002. Scanning surface confocal microscopy for simultaneous topographical and fluorescence imaging: application to single virus-like particle entry into a cell. *Proc. Natl. Acad. Sci. USA.* 99:16018–16023.
5. Mathur, A. B., G. A. Truskey, and W. M. Reichert. 2000. Atomic force and total internal reflection fluorescence microscopy for the study of force transmission in endothelial cells. *Biophys. J.* 78:1725–1735.
6. Nishida, S., Y. Funabashi, and A. Ikai. 2002. Combination of AFM with an objective-type total internal reflection fluorescence microscope (TIRFM) for nanomanipulation of single cells. *Ultramicroscopy.* 91: 269–274.
7. Axelrod, D. 2003. Total internal reflection fluorescence microscopy in cell biology. *Methods Enzymol.* 361:1–33.

8. Yamada, T., R. Afrin, H. Arakawa, and A. Ikai. 2004. High sensitivity detection of protein molecules picked up on a probe of atomic force microscope based on the fluorescence detection by a total internal reflection fluorescence microscope. *FEBS Lett.* 569:59–64.
9. Sarkar, A., R. B. Robertson, and J. M. Fernandez. 2004. Simultaneous atomic force microscope and fluorescence measurements of protein unfolding using a calibrated evanescent wave. *Proc. Natl. Acad. Sci. USA.* 101:12882–12886.
10. Pardee, J. D., and J. A. Spudich. 1982. Purification of muscle actin. *Methods Enzymol.* 85:164–182.
11. Margossian, S. S., and S. Lowey. 1982. Preparation of myosin and its subfragments from rabbit skeletal muscle. *Methods Enzymol.* 85: 55–72.
12. Kron, S. J., Y. Y. Toyoshima, T. Q. Uyeda, and J. A. Spudich. 1991. Assays for actin sliding movement over myosin-coated surfaces. *Methods Enzymol.* 196:399–416.
13. Kellermayer, M. S., and H. L. Granzier. 1996. Calcium-dependent inhibition of in vitro thin-filament motility by native titin. *FEBS Lett.* 380:281–286.
14. Grama, L., B. Somogyi, and M. S. Kellermayer. 2001. Global configuration of single titin molecules observed through chain-associated rhodamine dimers. *Proc. Natl. Acad. Sci. USA.* 98:14362–14367.
15. Kellermayer, M. S. Jr., T. R. Hinds, and G. H. Pollack. 1995. Persisting in vitro actin motility at nanomolar adenosine triphosphate levels: comparison of skeletal and cardiac myosins. *Physiol. Chem. Phys. Med. NMR.* 27:167–178.
16. Harada, Y., A. Noguchi, A. Kishino, and T. Yanagida. 1987. Sliding movement of single actin filaments on one-headed myosin filaments. *Nature.* 326:805–808.
17. Hutter, J. L., and J. Bechhoefer. 1993. Calibration of atomic-force microscope tips. *Rev. Sci. Instrum.* 64:1868–1873.
18. Proksch, R., T. E. Schäffer, D. P. Cleveland, R. C. Callahan, and M. B. Viani. 2004. Finite optical spot size and position corrections in thermal spring constant calibration. *Nanotechnology.* 15:1344–1350.
19. Walters, D. A., J. P. Cleveland, N. H. Thomson, H. G. Hansma, M. A. Wendman, G. Gurley, and V. Elings. 1996. Short cantilevers for atomic force microscopy. *Rev. Sci. Instrum.* 67:3583–3590.
20. Bustamante, C., J. F. Marko, E. D. Siggia, and S. Smith. 1994. Entropic elasticity of lambda-phage DNA. *Science.* 265:1599–1600.
21. Kellermayer, M. S., C. Bustamante, and H. L. Granzier. 2003. Mechanics and structure of titin oligomers explored with atomic force microscopy. *Biochim. Biophys. Acta.* 1604:105–114.
22. Rief, M., M. Gautel, F. Oesterhelt, J. M. Fernandez, and H. E. Gaub. 1997. Reversible unfolding of individual titin immunoglobulin domains by AFM. *Science.* 276:1109–1112.
23. Rief, M., F. Oesterhelt, B. Heymann, and H. E. Gaub. 1997. Single molecule force spectroscopy on polysaccharides by atomic force microscopy. *Science.* 275:1295–1297.
24. Lakowicz, J. R. 1983. Principles of Fluorescence Spectroscopy. Plenum Publishing, New York.
25. Lakowicz, J. R., H. Szmacinski, K. Nowaczyk, K. W. Berndt, and M. Johnson. 1992. Fluorescence lifetime imaging. *Anal. Biochem.* 202: 316–330.
26. Deniz, A. A., M. Dahan, J. R. Grunwell, T. Ha, A. E. Faulhaber, D. S. Chemla, S. Weiss, and P. G. Schultz. 1999. Single-pair fluorescence resonance energy transfer on freely diffusing molecules: observation of Forster distance dependence and subpopulations. *Proc. Natl. Acad. Sci. USA.* 96:3670–3675.
27. Ha, T., T. Enderle, D. F. Ogletree, D. S. Chemla, P. R. Selvin, and S. Weiss. 1996. Probing the interaction between two single molecules: fluorescence resonance energy transfer between a single donor and a single acceptor. *Proc. Natl. Acad. Sci. USA.* 93:6264–6268.
28. Horton, H., P. Lehenkari, and G. Charras. 2003. Combined atomic force and confocal microscopy for biological processes. *Microscopy and Analysis.* 86:17–19.
29. Micic, M., D. H. Hu, Y. D. Suh, G. Newton, M. Romine, and H. P. Lu. 2004. Correlated atomic force microscopy and fluorescence lifetime imaging of live bacterial cells. *Coll. Surf. B Biointerfaces.* 34: 205–212.
30. Burghardt, T. P., K. Ajtai, and J. Borejdo. 2006. In situ single-molecule imaging with attoliter detection using objective total internal reflection confocal microscopy. *Biochemistry.* 45:4058–4068.
31. Kellermayer, M. S., S. B. Smith, H. L. Granzier, and C. Bustamante. 1997. Folding-unfolding transitions in single titin molecules characterized with laser tweezers. *Science.* 276:1112–1116.
32. Tskhovrebova, L., J. Trinick, J. A. Sleep, and R. M. Simmons. 1997. Elasticity and unfolding of single molecules of the giant muscle protein titin. *Nature.* 387:308–312.
33. Forkey, J. N., M. E. Quinlan, M. A. Shaw, J. E. Corrie, and Y. E. Goldman. 2003. Three-dimensional structural dynamics of myosin V by single-molecule fluorescence polarization. *Nature.* 422:399–404.
34. Yildiz, A., J. N. Forkey, S. A. McKinney, T. Ha, Y. E. Goldman, and P. R. Selvin. 2003. Myosin V walks hand-over-hand: single fluorophore imaging with 1.5-nm localization. *Science.* 300:2061–2065.